The MYC-YBX1 Circuit in Maintaining Stem-like Vincristine-Resistant Cells in Rhabdomyosarcoma

Madeline Fritzke

Kenian Chen

Weiliang Tang

Spencer Stinson

Misa Ito

Lin Xu

Eleanor Chen (✉ eleanor2@uw.edu)

Abstract

Rhabdomyosarcoma (RMS) is a devastating pediatric soft tissue sarcoma with no effective therapy for relapsed disease. There is limited knowledge on the mechanisms underlying treatment failures. We demonstrated that treatment of RMS cells with vincristine led to an increase of CD133-positive stem-like resistant cells. By single cell RNAseq analysis, MYC and YBX1 were among the top-scored transcription factors in CD133-high expressing cells. CRISPR/Cas9-mediated targeting of *MYC* and *YBX1* reduced stem-like characteristics and viability of the vincristine-resistant cells. MYC and YBX1 exhibited mutual regulation with MYC binding to the *YBX1* promoter and YBX1 binding the *MYC* mRNA. A MYC inhibitor, MYC361i, synergized with vincristine to reduce tumor growth and deplete the stem-like cells in a zebrafish model of RMS. MYC and YBX expression showed positive correlation in RMS patients. High expression of *MYC* correlated with poor survival. Targeting the MYC-YBX1 axis represents a promising option for improving survival of RMS patients.

Introduction:

Rhabdomyosarcoma (RMS) is a devastating pediatric soft tissue sarcoma (250–300 cases a year in the US) [1,2] and consists of two major subtypes based on genetic alterations: fusion-negative (FN) and fusion-positive (FP). FN RMS is characterized by mutations in the receptor tyrosine kinase/RAS/PIK3CA axis in greater than 90% of cases [3]. In contrast, FP RMS is characterized by a translocation event resulting in the fusion between PAX3 or PAX7 and FOXO1 genes [4,5]. While localized disease of RMS can be controlled with surgery, chemotherapy and radiation, there is no effective treatment against relapsed or metastatic disease regardless of subtype, with less than 30% 3-year survival rate [6]. There is an urgent need to understand the biology underlying treatment failure in order to identify more effective therapy options for improving survival outcomes of treatment-refractory RMS.

To date, there are limited data on the molecular basis of chemotherapy resistance in RMS. A previous study has demonstrated survival of a cell subpopulation expressing *MYOD1* in an RMS cell line following treatment with standard-of-care chemotherapeutic agents, vincristine and doxorubicin [7]. Other studies have shown high levels of anti-apoptotic proteins are present in treatment-refractory RMS tumors [8,9] and up-regulation of selective signaling pathways (e.g. GP130/STAT and Hedgehog) in chemotherapy-resistant RMS cells [10,11]. Recently, the study by Patel et al demonstrates that chemotherapy eliminates proliferative myoblast-like cells in FN embryonal subtype of RMS (ERMS), leaving behind an immature cell population that recapitulates the paraxial mesodermal cells in development [12]. In all, previous findings suggest that there are transcriptional changes that alter cell state in proliferation and differentiation as RMS cells develop therapy resistance. However, the cellular and molecular mechanisms underlying early cell state adaptation leading to emergence of chemotherapy-resistant RMS cells remain unknown.

In this study, we aimed to characterize the cell state and molecular mechanisms underlying the biology of therapy-resistant RMS cells in response to treatment with the standard-of-care chemotherapeutic agent, vincristine.

Results:

Vincristine treatment generated a population of RMS cells with stem-like characteristics

To characterize the cellular characteristics and state of vincristine-resistant RMS cells, we treated a panel of FN and FP RMS cell lines (FN: RD and SMS-CTR; FP: Rh5 and Rh30) with a concentration of vincristine that killed 80−90% of cells (IC80-90) over 7 days. This treatment resulted in a population of slow-growing cells in comparison to the parental lines (Fig. 1A-E; Fig. S1A). These vincristine-resistant cells showed enlarged and irregular cell size with bizarre-shaped nuclei. By cell cycle analysis, vincristine-resistant cells showed a delay in cell cycle with increased number of cells in the quiescent G0/G1 phase and reduced number of cells in the proliferative S phase compared to the parental cells (Fig. 1F).

To assess whether vincristine treatment alters the cell state of the RMS cells, we showed that in comparison with the parental cells, FN RD and SMS-CTR cells following 7-day treatment of vincristine at IC 80−90 were enriched with CD133-positive cells on immunofluorescence (IF) (Fig. 1G-J). These cells also showed statistically significant up-regulation of stem cell markers, *CD133, PAX7*, *OCT4*, *NANOG* and *SOX2*, by quantitative RT-PCR (Unpaired t-test, $P < 0.01$, Fig. 1K).

FN RMS spheres enrich for CD133-expressing stem-like cells and show increased resistance to standard-of-care therapeutics

RMS spheres cultured in stem-cell media have previously been shown to be enriched for CD133-positive stem-like cells and are more resistant to the chemotherapeutics, cisplatin and chlorambucil [13]. Similarly, we showed that serially-passaged spheres derived from RD showed an increase in CD133 expression as well as CD133-expressing cells compared to the bulk xenograft tumor-derived from the RD line (ANOVA, *P* < 0.0001, Fig. S1 B-C). The spheres generated from the SMS-CTR cells also showed a similar increase in the CD133-expressing cells (Fig. S1 D). By contrast, the spheres generated from the two FP RMS lines (Rh5 and Rh30) lacked CD133-positive expressing cells (Fig. S1 D), suggesting that a different marker may better highlight the stem cell-like population in FP RMS cells. The spheres generated from both FN RMS cell lines (RD and SMS-CTR) and FP RMS cell lines (Rh5 and Rh30) treated with varying doses of the standard-of-care chemotherapeutic agent, vincristine, all exhibited decreased sensitivity compared to the parental adherent cells, as evidenced by ∼ 3 to 9-fold increase in IC50 (Fig. S1 E).

MYC and YBX1-driven transcriptional regulatory networks are up-regulated in CD133-positive stem-like RMS cells

As CD133-positive stem-like cells are enriched in the FN RMS spheres, we used serially passaging of RD sphere cells cultured in stem cell media to generate a sufficient number of CD133-positive cells for gene expression profiling by single cell RNA sequencing. Sphere cells harvested at passages 1 (P1) and 5 (P5) were subjected to processing and analysis by single cell RNA sequencing. As displayed by Uniform Manifold Approximation and Projection (UMAP) (Fig. 2A), both P1 and P5 RD sphere cells showed similar clustering patterns (clustering for P1 and P5 shown in Fig. 2A) with approximately 19 unique clusters identified. *CD133* (*PROM1*)-expressing cells showed relatively diffuse distribution throughout all clusters (Fig. 2B), indicating dynamic transcriptional plasticity of CD133-expressing cells. Through the enrichment analysis against TRRUST (Transcriptional Regulatory Relationships Unraveled by Sentence-based Text mining) database using Metascape, we observed that MYC and YBX1 are among the top-scored master transcription factors in *CD133*-high expressing RD cells compared to *CD133*-low expressing cells (Fig. 2C). Protein expression of MYC and YBX1 was also detected in serially passaged spheres by immunohistochemistry (RD P5 spheres shown in Fig. 2D) with MYC showing nuclear localization and YBX1 showing cytoplasmic localization. In addition, we found stronger correlations between MYC and YBX1, MYC and MYC target genes as well as between YBX and YBX1-target genes, in CD133-high expressing sphere cells in comparison with CD133-low expressing cells (Fig. 2E, 2F ; Fig. S2 A-C). Up-regulation of well-known downstream targets genes of MYC and YBX1 was noted in CD133-high expressing RD cells (Fig. 2D-E), which were independently validated on RD sphere cells using quantitative RT-PCR (Fig. S2 D).

Targeted disruption of MYC and YBX1 inhibits tumor RMS tumor cell growth and sphere formation and induces cell death in CD133-positive stem-like cells

To assess the loss-of-function effects of MYC and YBX1 on RMS tumor cell growth and sphere formation, FN RMS (RD, SMS-CTR) and FP RMS (Rh5 and Rh30) Cas9-expressing stable lines were transduced with lentiviral constructs expressing double gRNAs (dgRNA) against *MYC* and *YBX1*. CRISPR/Cas9-mediated disruption of *MYC* and *YBX1* (Fig. 3A; Fig. S3 A) inhibited cell growth by cell counts and CellTiter-Glo viability assays (Fig. 3B; Fig. S3 B) as well as reduced sphere formation frequency and size at two cell dilutions (Fig. 3C-G; Fig. S3 C-D). To demonstrate gene targeting specificity, we showed that overexpression of Cas9-resistant MYC and YBX1 alleviated the cell growth defect resulted from CRISPR/Cas9-mediated gene targeting of *MYC* and *YBX1*, respectively (Fig. S3 E).

To assess the effect of *MYC* and *YBX1* gene disruption on the viability of CD133-positive sphere cells real-time, we generated a CD133:GFP SMS-CTR reporter line by knocking in the GFP cassette in frame with the CD133 locus via CRISPR/Cas9. By live imaging of dissociated sphere cells derived from the CD133:GFP SMS-CTR stained with the fluorogeneic NucView®530 Caspase-3 substrate 5 days following lentiviral transduction of the CRISPR dgRNA constructs and antibiotic selection, we observed an increased number of cells undergoing apoptosis including the CD133-positive cells (indicated by arrowheads in Fig. 3H; quantitation in Fig. S3 F, ANOVA, $P < 0.001$). Together, *MYC*- and *YBX1*-targeted disruption decreased stem-like characteristics of RMS cells and contributed to increased apoptosis in the CD133-positive stem-like cell population at least in FN RMS.

MYC and YBX1 play an important role in modulating chemosensitivity of the RMS cells

Given that MYC and YBX1 are essential for the viability of the CD133-positive stem-like FN RMS cells, and short-term vincristine-treated FN RMS-resistant cells have shown an increase in CD133-positive stem-like cells, we next asked whether MYC and YBX1 play a role in modulating chemosensitivity of FN RMS cells to vincristine. We first showed by quantitative RT-PCR that there was a relative increase in expression of *MYC* and *YBX1* in the resistant RD and SMS-CTR cells following 7-day treatment of vincristine at IC 80− 90 compared to vehicle (DMSO)-treated parental cells (Unpaired t-test, $P < 0.01$, Fig. 4A). To assess whether YBX1 and MYC are essential for the viability of resistant FN RMS cells following a short-term treatment with vincristine at IC 80−90, we transduced the Cas9-expressing RD cells that survived 7-day treatment of vincristine at IC80-90 with gene-specific double gRNAs (dgRNAs) and re-started vincristine treatment following transduction and antibiotic selection (schematic in Fig. 4B). While the vincristine-treated cells with targeted disruption of a safe-harbor genomic region targeting as a control remained relatively tolerant to the vincristine compared to the parental cells, targeted disruption of *MYC* and *YBX1* reduced cell growth and increased cell death in the vincristine-treated cells (ANOVA, $P < 0.05$, Fig. 4B-D and Fig. S4 A). In addition, we generated RD and SMS-CTR resistant cells following a long-term treatment with incremental increase in vincristine concentration until a 5-10-fold increase in the IC50 compared to the parental cells (~ 9 months duration). In contrast to short-term treatment of vincristine, which generated resistant cells in predominantly dormant G0 state (Fig. 1F), long-term treatment of vincristine generated RD and SMS-CTR cells that showed cell cycle re-entry from G0 with delay in the G2-M phase (Fig. S4 C). CRISPR/Cas9-mediated targeted disruption of *MYC* and *YBX1* in these resistant cells generated from long-term exposure of vincristine also showed reduced growth compared to safe-harbor region-targeted control resistant cells (data for RD in Fig. 4E, ANOVA, $P < 0.05$), indicating that MYC and YBX1 play an important role in maintaining the viability of vincristine-resistant FN RMS cells over time.

To assess whether MYC or YBX1 overexpression can confer tolerance to vincristine treatment on RMS cells, we showed that overexpression of MYC but not YBX1 in the Rh30 FP RMS line with low MYC expression conferred increased tolerance to vincristine in a dose-dependent manner (ANOVA, $P < 0.0005$, Fig. 4F).

Reciprocal regulation of MYC and YBX1 in FN RMS cells

Given the role of MYC in gene transcription and the DNA and RNA-binding capacity of YBX1, we next asked whether MYC and YBX1 showed mutual regulation at the transcriptional or post-transcriptional level. We first observed that upon targeted disruption of *MYC* in two FN RMS lines, RD and SMS-CTR, there was reduced mRNA expression of *YBX1* by quantitative RT-PCR and protein expression by Western blot analysis (Fig. 3A, Fig. S3 A and Fig. 5A-B). Similarly, targeted disruption of *YBX1* in RD and SMS-CTR cells also reduced *MYC* mRNA and protein expression (Fig. 3A and Fig. 5A-B).

To assess whether MYC regulates expression of *YBX1* at the level of transcription, we showed by the CUT and RUN assay performed on the RD and SMS-CTR cells treated with vincristine that MYC bound to the promoter containing the consensus MYC binding motif (CACGTG) of YBX1, CD133 and muscle satellite/RMS tumor propagating cell markers, MYF5 and PAX7 (Fig. 5C-D). YBX1 was expressed in the cytoplasm in RMS cells (Fig. 2D), suggesting its functional role at the post-transcriptional level. To assess whether YBX1 binds to the *MYC* mRNA, we demonstrated the YBX1 protein-*MYC* mRNA interaction by the RNA immunoprecipitation assay (RIP) performed on RD cells using the antibody against YBX1 in the RNA pull down and primers against the 3' UTR region of *MYC* mRNA (Fig. 5E).

Overall, the findings indicate that MYC and YBX show reciprocal regulation with MYC regulating gene expression of *YBX1*, and YBX1 regulating mRNA stability of *MYC*.

The combination treatment of the MYC inhibitor, MYCi361, and vincristine significantly inhibits RMS tumor cell growth and depletes stem-like cell subpopulation in vivo.

MYCi361 is a MYC inhibitor previously described by Han et al to decrease MYC protein activity by disrupting MYC/MAX dimer formation and impairing MYC-driven gene expression [14]. We showed in cultured RD and SMS-CTR cells that treatment with the combination of MYCi361 and vincristine significantly reduced cell growth compared to treatment with each agent alone (Fig. S5 A). By quantitative RT-PCR, MYCi361-treated RD and SMS-CTR cells showed decreased expression levels of known MYC target genes (Fig. S5 B). To assess whether MYCi361 could be a potential therapeutic agent in combination with vincristine to reduce RMS tumor cell growth *in vivo*, we tested the two-agent combination in the KRAS(G12D)-induced zebrafish FN RMS model. Primary zebrafish RMS tumor cells expressing a transgenic (*rag2*:dsRed) fluorescent reporter were transplanted into a pool of syngeneic CG1-strain host zebrafish, engrafted tumor fish were treated with DMSO (vehicle control), MYCi361 (100 mg/kg), vincristine (0.4 mg/kg) or MYCi361 and vincristine in combination with half the dosage for each drug for 7 days. The dosage of MYCi361 and vincristine was titrated to a level that only slightly affected tumor growth as a single agent *in vivo*. We observed that treatment of zebrafish RMS tumors with the combination of vincristine and MYCi361 significantly reduced tumor growth compared to the tumors treated with vincristine or MYCi361 alone (Fig. 6A-B). This was supported by a significantly greater decrease in the proliferative index and increase in the number of apoptotic cells in tumors treated with the two-drug combination, as highlighted by immunohistochemistry for Ki67 and Caspase-3, respectively (see representative tumor sections from each treatment cohort and quantitative results in Fig. 6C-D).

To assess whether MYCi361 modulates the relative proportions of tumor cell subpopulations based on their differentiation status, we took advantage of the *myf5:GFP/mylz2:mCherry* transgenic zebrafish line to label distinct cell subpopulations of FN RMS based on their differentiation status *in vivo* [15]. The *myf5*:GFP+/*mylz2*:mCherry-negative (G + R-) stem cell-like tumor-propagating-cell (TPC) population has been shown to have self-renewal capacity while late-differentiating *myf5*:GFP-negative/*mylz2*:mCherry + tumor cells (G-R+) lack the capacity to self-renew [15,16]. Following 7-day drug treatment of fish-bearing engrafted *myf5*:GFP/*mylz2*:mCherry expressing RMS tumors, relative proportions of cell subpopulations

were assessed by Fluorescence Activated Cell Sorting (FACS) (n = 3 independent tumors). The treatment with MYCi361 resulted in significant depletion in the proportion of the *myf5*:GFP+/*mylz2*:mCherry-negative TPC population and a concomitant increase in the proportion of *myf5*:GFP-negative/*mylz2*:mCherry + late-differentiating cells (Representative flow cytometric analysis and quantitation of cell subpopulations in Fig. 6E-F; p < 0.05), MYCi361-treated tumor cells also showed decreased expression of stem genes, *pax7* and *myf5* (Fig. S5 C).

High MYC expression correlates with poor survival outcomes of FN RMS.

To assess whether MYC and YBX1 expression could be detected in recurrent or metastatic RMS samples, we assessed by immunohistochemistry protein expression of MYC and YBX1 in a tissue microarray of tissue cores from 32 RMS patients, including 17 primary tumors (12 FN and 5 FP) and 15 recurrent or metastatic tumors (8 FN and 7 FP) along with 5 muscle controls. FN samples include ERMS (n = 9), FN ARMS (n = 2) and spindle cell/sclerosing variant (n = 1). MYC and YBX1 were expressed in at least a subset of primary RMS samples (MYC: 3 of 9 (33%) in FN RMS, 1 of 5 (20%) in FP RMS; YBX1: 12 of 12 (100%) in FN RMS, 5 of 5 (100%) in FP RMS) as well as recurrent/metastatic RMS samples (MYC: 4 of 8 (50%) in FN RMS, 1 of 7 (14.3%) in FP RMS; YBX1: 8 of 8 (100%) in FN RMS, 7 of 7 (100%) in FP RMS). MYC staining showed a patchy distribution, while YBX1 staining showed a diffuse distribution (Fig. 7A). All normal muscle tissue samples were negative for both MYC and YBX1 (Fig. 7A). In all, MYC showed a trend of increased frequency of positive expression in recurrent/metastatic FN RMS, and YBX1 was expressed in all primary and metastatic FN and FP RMS tumor tissue samples examined (Fig. 7B), suggesting that MYC and YBX1 play a role in both primary and recurrent/metastatic RMS tumors.

To examine potential roles of *MYC* and *YBX* as biomarkers for RMS patients, we studied *MYC* or *YBX* mRNA expression in 81 RMS cases with survival data (63 fusion-negative and 18 fusion-positive). we first showed that high expression of *MYC* correlated positively with high expression of *YBX1* in both FN and FP patients, separately (Fig. 7C-D). We then asked whether *MYC* or *YBX1* expression in RMS tumors associated with patients' survival. Kaplan−Meier curves were generated based on gene expression values dichotomized into over- and under-expressed groups using the median expression value within each cohort as a cutoff. However, while expression of *YBX* did not correlate with overall survival, high expression of *MYC* correlated with decreased overall survival in the FN RMS patients (Fig. 7E, log-rank test, p = 0.043, HR = 2.08, 95% CI = 1.04−4.51) but not the FP RMS cases (Fig. 7F, p = 0.673, HR = 1.46, 95% CI = 0.25−8.48). Although the small sample size in both subsets compromises the ability to draw firm conclusions, the findings suggest that expression of *MYC* might be useful as a clinical prognostic biomarker if they are confirmed in a prospective analysis.

Discussion:

MYC is a regulatory transcription factor with essential roles in regulating embryonic stem cell identity and various aspects of cancer biology including proliferation, growth, metabolism and differentiation [17−20]. MYC has also been shown in a few cancer types as one of master transcription factors to control cell

phenotypes or identities. For example, in breast cancer, MYC-driven epigenetic reprogramming causes activation of de novo enhancer to support dedifferentiation and onset of a stem-like state while repressing transcriptional activity of lineage-specifying transcription factors [17]. In pancreatic ductal adenocarcinoma, MYC binds to neuroendocrine genes to facility ductal-neuroendocrine plasticity and thereby contributes to chemotherapy resistance [21]. Our study demonstrated MYC binding to the E-box DNA response element within the promoters/enhancers of stem genes in FN RMS, and disruption of MYC activity by either CRISPR/Cas9 gene targeting or treatment with the MYC inhibitor, MYCi361, reduced stem-like characteristics and increased apoptosis of vincristine-resistant FN RMS cells. The findings suggest that MYC-driven transcriptional regulation plays an important role in modulating stem cell state plasticity of the resistant cells in response to the treatment with vincristine. The study by Patel et al. demonstrates that RMS tumors recapitulate the spectrum of embryonic myogenesis, and following chemotherapy treatment, the immature population that resembles embryonic paraxial mesoderm expands to replace the proliferative myoblast-like cells. Together, chemotherapy resistance in RMS likely arises from cell state plasticity in treated tumors cells with a shift towards a more stem-like or immature embryonic phenotype. The molecular mechanisms by which MYC and other transcription factors drive the dynamics of cell state plasticity over time in response to vincristine treatment remain to be further investigated.

Our study demonstrated that MYC and YBX1-drvien transcriptional regulatory networks were enriched in the CD133-high stem cell population in FN RMS. YBX1 is a DNA and RNA-binding protein with diverse functions in transcriptional and post-transcriptional regulation [22,23]. In our study, targeted disruption of *YBX1* also phenocopied the loss-of-function effects of MYC on the viability of CD133-positive RMS stem cell population and the stem cell-enriched vincristine-resistant cells. Mechanistically, MYC promoted transcriptional activity of *YBX1* by binding to the E-box motif in the *YBX1* promoter. YBX1 in turn binds to the *MYC* mRNA to regulate its stability. To date, there has been only a few studies characterizing the MYC-YBX1 interaction in cancer. The mutual regulation of the MYC-YBX1 circuit has only been described so far in multiple myeloma, where the perturbation of the MYC-YBX1 circuit induces apoptosis in multiple myeloma cells [24]. YBX1 has been shown to either promote or decrease *MYC* mRNA stability. Specifically, YBX1 binds to a long non-coding RNA (Linc2042) in squamous cell carcinoma to facilitate tumor cell growth and metastasis [25]. In contrast, YBX1 promotes mRNA decay of *MYC* in an m6A-dependent manner to maintain the viability of acute myeloid leukemia cells [26]. In our study, the regulatory loop of MYC-YBX1 results in increased MYC mRNA stability and YBX1 gene expression, which is a novel mechanism for maintaining the viability of the stem-like vincristine-resistant cells. Whether the MYC-YBX1 circuit plays a role in the progression to therapy resistance in other cancer types remains to be further investigated.

MYC, similar to many other transcription factors, lacks a deep surface binding pocket, thereby making drug design challenging. So far, a MYC-derived bHLH-zipper domain peptide, Omomyc, and JQ1, a small molecular inhibitor of the Bromodomain and Extraterminal (BET) protein, BRD4, have been shown to have the robust capacity in suppressing the transcriptional activity of MYC [27,28], In this study, we showed that

the small molecule MYC inhibitor, MYCi361, which was recently shown by Han et al, to directly inhibit MYC activity [14], sensitized FN RMS cells to vincristine treatment *in vitro* and in the zebrafish model *in vivo*. The combination of MYCi361 and vincristine significantly reduced RMS tumor growth and the stem cell-like tumor propagating cell population. In addition, there was a positive correlation between *MYC* and *YBX1* expression levels in RMS patients, and high *MYC* expression levels correlated with poorer survival outcomes in our analysis of 81 RMS patients. Our findings indicate that targeting MYC or MYC-driven transcriptional network is a promising therapeutic option for reducing the likelihood of chemotherapy resistance in RMS and maybe a useful clinical prognostic biomarker if our findings are confirmed in a larger-scale prospective analysis.

In summary, our study has shown that vincristine-treatment of ERMS cells resulted in a stem-like resistant population that showed up-regulation of genes regulated by MYC and YBX1. The MYC-YBX1 mutual regulatory circuit contributed to the viability and maintenance of the vincristine-resistant cells. Targeting the MYC-YBX1 axis is a promising therapeutic option for reducing the therapy resistance in RMS.

Methods:

CRISPR/Cas9 Gene Targeting in Human RMS Cell Lines

Single knockout was accomplished by transducing RMS cells with lentiviral virus expressing safe-harbor control[29] or gene-specific double gRNAs (Table S1) and Cas9. Cells transduced with lentivirus were plated for cell-based assays following antibiotic selection 5 days post-transduction. Cloning of Cas9 and gRNA expression vectors was performed as described previously [29].

The coding portions of *MYC* and *YBX1* were amplified from the plasmids [30] obtained from Addgene (Watertown, MA) for cloning purposes. Silent mutations to alter PAM sites to create Cas9-resistant MYC lentiviral overexpression construct used in rescue and overexpression experiments were introduced using a 4-piece Gibson cloning strategy. YBX1 gRNAs were designed against non-coding regions of *YBX1*, so the coding portion was not altered in the lentiviral *YBX1* overexpression construct. All cell lines were previously authenticated by STR profiling and tested for mycoplasma contamination.

Single Cell RNA Sequencing (sci-RNA-seq3 Protocol)

RMS spheres were fixed in 4% paraformaldehyde and frozen liquid nitrogen prior to nuclear extraction. The samples were subsequently submitted to the single cell services at the Brotman Baty Institute for Precision Medicine (University of Washington) for single cell RNA library preparation and sequencing.

Pre-Processing of Single Cell RNA Sequencing Data

Base calls from sequencing were converted into fastq format using Illumina's bcl2fastq program and demultiplexed by University of Washington sequencing core. Reads were adaptor-clipped using trim_galore with default settings. Trimmed reads were mapped to the human reference genome (GRch38) using STAR program (version 2.5.2b). Uniquely mapping reads were extracted and duplicates were

removed based on unique molecular identifier (UMI) sequence. To generate expression matrices, the number of UMIs for each cell mapping to the exonic and intronic regions of each gene were calculated. Potential ambient RNA reads were estimated and removed using R package SoapX. Doublets were then identified using python package Scrublet [31]. Further analysis for quality filtering was performed using the Seurat R package (version 3.2.2). Only cells with total read count < 10000 and number of genes detected > 100 were kept. To remove potential dead cells from the analysis, cells with > 15% mitochondrial reads were filtered out. In total, we obtained 82133 cells from 4 conditions.

Integrated Analysis of Single Cell RNA Datasets

To account for potential batch effects, we performed an integrate analysis using the IntegrateData function implemented in Seurat package (version 3.2.2). Briefly, we performed data normalization using NormalizeData function and identified top variable genes using FindVariableFeatures. We then selected integration features and anchors using function SelectIntegrationFeatures and FindIntegrationAnchors respectively. Finally we passed the anchors to IntegrateData function and used dimension 50 to generate integrated Seurat objects.

Visualization and Clustering

For data visualization, we used Uniform Manifold Approximation and Projection (UMAP) to project cells on 2D space. Using graph-based clustering, we clustered the cells into 20 clusters using the FindCluster function in Seurat with resolution 0.3.

Imputation of Single Cell RNAseq Data and Enrichment Analysis

To categorize cells into CD133 high and CD133 low cells, we used Markov affinity-based graph imputation of cells (MAGIC) to denoise cell count matrix and fill in missing values to overcome dropout problem that is faced by current single cell technology. According to imputed CD133 expression levels, cells were designated as CD133 high/low cells if its expression level was in top 1/3 or bottom 1/3 of the condition (P1/P5), separately. Differential expressed genes comparing CD133-high and CD133-low cell populations were identified using Wilcoxon rank sum test implement in Seurat FindMarkers function.

Drug Treatment Studies and Assessment of Tumor Growth Using Zebrafish RMS Model

Zebrafish were maintained in a shared facility at the University of Washington under protocol #4330-01 approved by the University of Washington Subcommittee on Research Animal Care. Primary tumors *rag2:KRASG12D-T2A-GFP* were expanded by transplantation into 3−4 syngeneic adult CG1 fish. Tumor cells were then harvested by dissection and dissociation. For drug treatment studies, tumor cells were first transplanted subcutaneously into the peritoneal cavity at 20,000 cell per fish. Drug treatment study was performed on engrafted tumor bearing tumor fish ~ 10 days post-transplantation for 7 days. Drugs reconstituted in DMSO, vincristine (Sigma Aldrich) at 8 mg/kg and MYCi361 (100 mg/kg), and vehicle

(DMSO) were delivered on day 0 and day 4 in 5-microliter volume using a Hamilton syringe needle via the intraperitoneal route. Imaging of tumor-bearing fish at day 0 and day 7 was performed using a Nikon fluorescent dissecting scope. The tumor volume change was quantified using the ImageJ software as previously described [32].

Cell-based Assays

Cell counts, CellTiter-Glo assay, sphere and flow cytometry assays were performed based on the protocols previously described (18, 39). See additional details in Supplemental Methods.

CUT&RUN Assay

The CUT&RUN assay was performed using the EpiNext™ CUT&RUN Fast Kit per manufacturer's instructions. Approximately 10,000 cells were used for each reaction. The rabbit monoclonal MYC antibody (clone E5Q6W; Cell Signaling, Danvers, MA) and non-immune IgG as supplied in the kit were used in the chromatin capture reaction. The primers were for PCR verification are listed in Table S1.

RNA-Binding Protein Immunoprecipitation Assay

The RNA-binding protein immunoprecipitation assay was performed using the Magna RIP kit (Millipore) per manufacturer's instructions. The rabbit polyclonal anti-YBX1(1:100; clone D299; Cell Signaling, Danvers, MA) and negative control Rabbit IgG were used in the immunoprecipitation step. The primers used to detect MYC mRNA transcript are listed in Table S1.

Survival Association Analysis in RMS patient cohort

The 81 RMS cases with survival and gene expression data were published previously [33]. Cox proportional hazards model was used to calculate the statistical significance, as well as hazard ratios and 95% confidence intervals of the associations between the gene expression and survival. Kaplan-Meier curves were generated based on gene expression values dichotomized into over- and under-expressed groups using the within cohort median expression value as a cutoff.

Statistics

Two-tailed t-test and one-way/two-way ANOVA tests were used to assess statistical significance in differences between experimental and control samples when appropriate. A p value < 0.05 was considered statistically significant.

Additional details for immunohistochemistry, immunofluorescence, Western blots and quantitative RT-PCR are in Supplemental Methods.

Declarations

ACKNOWLEDGEMENT:

References

1. Amer, K.M., Thomson, J.E., Congiusta, D., Dobitsch, A., Chaudhry, A., Li, M., Chaudhry, A., Bozzo, A., Siracuse, B., Aytekin, M.N., et al. (2019). Epidemiology, Incidence, and Survival of Rhabdomyosarcoma Subtypes: SEER and ICES Database Analysis. Journal of Orthopaedic Research *37*, 2226–2230. 10.1002/jor.24387.

2. Wang, X., Feng, J., Li, Z., Zhang, X., Chen, J., and Feng, G. (2020). Characteristics and prognosis of embryonal rhabdomyosarcoma in children and adolescents: An analysis of 464 cases from the SEER database. Pediatr Investig *4*, 242–249. 10.1002/ped4.12220.

3. Shern, J.F., Chen, L., Chmielecki, J., Wei, J.S., Patidar, R., Rosenberg, M., Ambrogio, L., Auclair, D., Wang, J., Song, Y.K., et al. (2014). Comprehensive genomic analysis of rhabdomyosarcoma reveals a landscape of alterations affecting a common genetic axis in fusion-positive and fusion-negative tumors. Cancer discovery *4*, 216–231. 10.1158/2159–8290.CD-13-0639.

4. Barr, F.G., Galili, N., Holick, J., Biegel, J.A., Rovera, G., and Emanuel, B.S. (1993). Rearrangement of the PAX3 paired box gene in the paediatric solid tumour alveolar rhabdomyosarcoma. Nat Genet *3*, 113–117. 10.1038/ng0293-113.

5. Davis, R.J., D'Cruz, C.M., Lovell, M.A., Biegel, J.A., and Barr, F.G. (1994). Fusion of PAX7 to FKHR by the variant t(1;13)(p36;q14) translocation in alveolar rhabdomyosarcoma. Cancer Res *54*, 2869–2872.

6. Skapek, S.X., Ferrari, A., Gupta, A.A., Lupo, P.J., Butler, E., Shipley, J., Barr, F.G., and Hawkins, D.S. (2019). Rhabdomyosarcoma. Nat Rev Dis Primers *5*, 1. 10.1038/s41572-018-0051-2.

7. Dawson, L.E., D'Agostino, L., Hakim, A.A., Lackman, R.D., Brown, S.A., Sensenig, R.B., Antonello, Z.A., and Kuzin, I.I. (2020). Induction of Myogenic Differentiation Improves Chemosensitivity of Chemoresistant Cells in Soft-Tissue Sarcoma Cell Lines. Sarcoma *2020*, 8647981. 10.1155/2020/8647981.

8. Alcon, C., Manzano-Muñoz, A., Prada, E., Mora, J., Soriano, A., Guillén, G., Gallego, S., Roma, J., Samitier, J., Villanueva, A., et al. (2020). Sequential combinations of chemotherapeutic agents with BH3 mimetics to treat rhabdomyosarcoma and avoid resistance. Cell Death Dis *11*, 634. 10.1038/s41419-020-02887-y.

9. Manzella, G., Moonamale, D.C., Römmele, M., Bode, P., Wachtel, M., and Schäfer, B.W. (2021). A combinatorial drug screen in PDX-derived primary rhabdomyosarcoma cells identifies the NOXA -

BCL-XL/MCL-1 balance as target for re-sensitization to first-line therapy in recurrent tumors. Neoplasia *23*, 929–938. 10.1016/j.neo.2021.07.001.

10. Wu, X., Xiao, H., Wang, R., Liu, L., Li, C., and Lin, J. (2016). Persistent GP130/STAT3 Signaling Contributes to the Resistance of Doxorubicin, Cisplatin, and MEK Inhibitor in Human Rhabdomyosarcoma Cells. Curr Cancer Drug Targets *16*, 631–638. 10.2174/1568009615666150916093110.

11. Yoon, J.W., Lamm, M., Chandler, C., Iannaccone, P., and Walterhouse, D. (2020). Up-regulation of GLI1 in vincristine-resistant rhabdomyosarcoma and Ewing sarcoma. BMC Cancer *20*, 511. 10.1186/s12885-020-06985-0.

12. Patel, A.G., Chen, X., Huang, X., Clay, M.R., Komorova, N., Krasin, M.J., Pappo, A., Tillman, H., Orr, B.A., McEvoy, J., et al. (2022). The myogenesis program drives clonal selection and drug resistance in rhabdomyosarcoma. Dev Cell *57*, 1226–1240.e8. 10.1016/j.devcel.2022.04.003.

13. Walter, D., Satheesha, S., Albrecht, P., Bornhauser, B.C., D'Alessandro, V., Oesch, S.M., Rehrauer, H., Leuschner, I., Koscielniak, E., Gengler, C., et al. (2011). CD133 positive embryonal rhabdomyosarcoma stem-like cell population is enriched in rhabdospheres. PLoS One *6*, e19506. 10.1371/journal.pone.0019506.

14. Han, H., Jain, A.D., Truica, M.I., Izquierdo-Ferrer, J., Anker, J.F., Lysy, B., Sagar, V., Luan, Y., Chalmers, Z.R., Unno, K., et al. (2019). Small-Molecule MYC Inhibitors Suppress Tumor Growth and Enhance Immunotherapy. Cancer Cell *36*, 483–497.e15. 10.1016/j.ccell.2019.10.001.

15. Ignatius, M.S., Chen, E., Elpek, N.M., Fuller, A.Z., Tenente, I.M., Clagg, R., Liu, S., Blackburn, J.S., Linardic, C.M., Rosenberg, A.E., et al. (2012). In vivo imaging of tumor-propagating cells, regional tumor heterogeneity, and dynamic cell movements in embryonal rhabdomyosarcoma. Cancer cell *21*, 680–693. 10.1016/j.ccr.2012.03.043.

16. Chen, E.Y., DeRan, M.T., Ignatius, M.S., Grandinetti, K.B., Clagg, R., McCarthy, K.M., Lobbardi, R.M., Brockmann, J., Keller, C., Wu, X., et al. (2014). Glycogen synthase kinase 3 inhibitors induce the canonical WNT/beta-catenin pathway to suppress growth and self-renewal in embryonal rhabdomyosarcoma. Proc Natl Acad Sci U S A *111*, 5349–5354. 10.1073/pnas.1317731111.

17. Poli, V., Fagnocchi, L., Fasciani, A., Cherubini, A., Mazzoleni, S., Ferrillo, S., Miluzio, A., Gaudioso, G., Vaira, V., Turdo, A., et al. (2018). MYC-driven epigenetic reprogramming favors the onset of tumorigenesis by inducing a stem cell-like state. Nat Commun *9*, 1024. 10.1038/s41467-018-03264-2.

18. Sancho, P., Burgos-Ramos, E., Tavera, A., Bou Kheir, T., Jagust, P., Schoenhals, M., Barneda, D., Sellers, K., Campos-Olivas, R., Graña, O., et al. (2015). MYC/PGC-1α Balance Determines the Metabolic Phenotype and Plasticity of Pancreatic Cancer Stem Cells. Cell Metab *22*, 590–605. 10.1016/j.cmet.2015.08.015.

19. Fagnocchi, L., and Zippo, A. (2017). Multiple Roles of MYC in Integrating Regulatory Networks of Pluripotent Stem Cells. Front Cell Dev Biol *5*, 7. 10.3389/fcell.2017.00007.

20. Kim, J., Woo, A.J., Chu, J., Snow, J.W., Fujiwara, Y., Kim, C.G., Cantor, A.B., and Orkin, S.H. (2010). A Myc network accounts for similarities between embryonic stem and cancer cell transcription programs. Cell *143*, 313–324. 10.1016/j.cell.2010.09.010.

21. Farrell, A.S., Joly, M.M., Allen-Petersen, B.L., Worth, P.J., Lanciault, C., Sauer, D., Link, J., Pelz, C., Heiser, L.M., Morton, J.P., et al. (2017). MYC regulates ductal-neuroendocrine lineage plasticity in pancreatic ductal adenocarcinoma associated with poor outcome and chemoresistance. Nat Commun *8*, 1728. 10.1038/s41467-017-01967-6.

22. Kuwano, M., Shibata, T., Watari, K., and Ono, M. (2019). Oncogenic Y-box binding protein-1 as an effective therapeutic target in drug-resistant cancer. Cancer Sci *110*, 1536–1543. 10.1111/cas.14006.

23. Kwon, E., Todorova, K., Wang, J., Horos, R., Lee, K.K., Neel, V.A., Negri, G.L., Sorensen, P.H., Lee, S.W., Hentze, M.W., et al. (2018). The RNA-binding protein YBX1 regulates epidermal progenitors at a posttranscriptional level. Nat Commun *9*, 1734. 10.1038/s41467-018-04092-0.

24. Bommert, K.S., Effenberger, M., Leich, E., Küspert, M., Murphy, D., Langer, C., Moll, R., Janz, S., Mottok, A., Weissbach, S., et al. (2013). The feed-forward loop between YB-1 and MYC is essential for multiple myeloma cell survival. Leukemia *27*, 441–450. 10.1038/leu.2012.185.

25. Du, J., Zhang, G., Qiu, H., Yu, H., and Yuan, W. (2020). A novel positive feedback loop of linc02042 and c-Myc mediated by YBX1 promotes tumorigenesis and metastasis in esophageal squamous cell carcinoma. Cancer Cell Int *20*, 75. 10.1186/s12935-020-1154-x.

26. Feng, M., Xie, X., Han, G., Zhang, T., Li, Y., Li, Y., Yin, R., Wang, Q., Zhang, T., Wang, P., et al. (2021). YBX1 is required for maintaining myeloid leukemia cell survival by regulating BCL2 stability in an m6A-dependent manner. Blood *138*, 71–85. 10.1182/blood.2020009676.

27. Delmore, J.E., Issa, G.C., Lemieux, M.E., Rahl, P.B., Shi, J., Jacobs, H.M., Kastritis, E., Gilpatrick, T., Paranal, R.M., Qi, J., et al. (2011). BET bromodomain inhibition as a therapeutic strategy to target c-Myc. Cell *146*, 904–917. 10.1016/j.cell.2011.08.017.

28. Soucek, L., Jucker, R., Panacchia, L., Ricordy, R., Tatò, F., and Nasi, S. (2002). Omomyc, a potential Myc dominant negative, enhances Myc-induced apoptosis. Cancer Res *62*, 3507–3510.

29. Phelps, M.P., Bailey, J.N., Vleeshouwer-Neumann, T., and Chen, E.Y. (2016). CRISPR screen identifies the NCOR/HDAC3 complex as a major suppressor of differentiation in rhabdomyosarcoma. Proc Natl Acad Sci U S A. 10.1073/pnas.1610270114.

30. Kawaguchi, Y., Kovacs, J.J., McLaurin, A., Vance, J.M., Ito, A., and Yao, T.P. (2003). The deacetylase HDAC6 regulates aggresome formation and cell viability in response to misfolded protein stress. Cell *115*, 727–738. 10.1016/s0092-8674(03)00939-5.

31. Wolock, S.L., Lopez, R., and Klein, A.M. (2019). Scrublet: Computational Identification of Cell Doublets in Single-Cell Transcriptomic Data. Cell Syst *8*, 281–291.e9. 10.1016/j.cels.2018.11.005.

32. Vleeshouwer-Neumann, T., Phelps, M., Bammler, T.K., MacDonald, J.W., Jenkins, I., and Chen, E.Y. (2015). Histone Deacetylase Inhibitors Antagonize Distinct Pathways to Suppress Tumorigenesis of Embryonal Rhabdomyosarcoma. PLoS One *10*, e0144320. 10.1371/journal.pone.0144320.

33. Xu, L., Zheng, Y., Liu, J., Rakheja, D., Singleterry, S., Laetsch, T.W., Shern, J.F., Khan, J., Triche, T.J., Hawkins, D.S., et al. (2018). Integrative Bayesian Analysis Identifies Rhabdomyosarcoma Disease Genes. Cell Rep *24*, 238–251. 10.1016/j.celrep.2018.06.006.
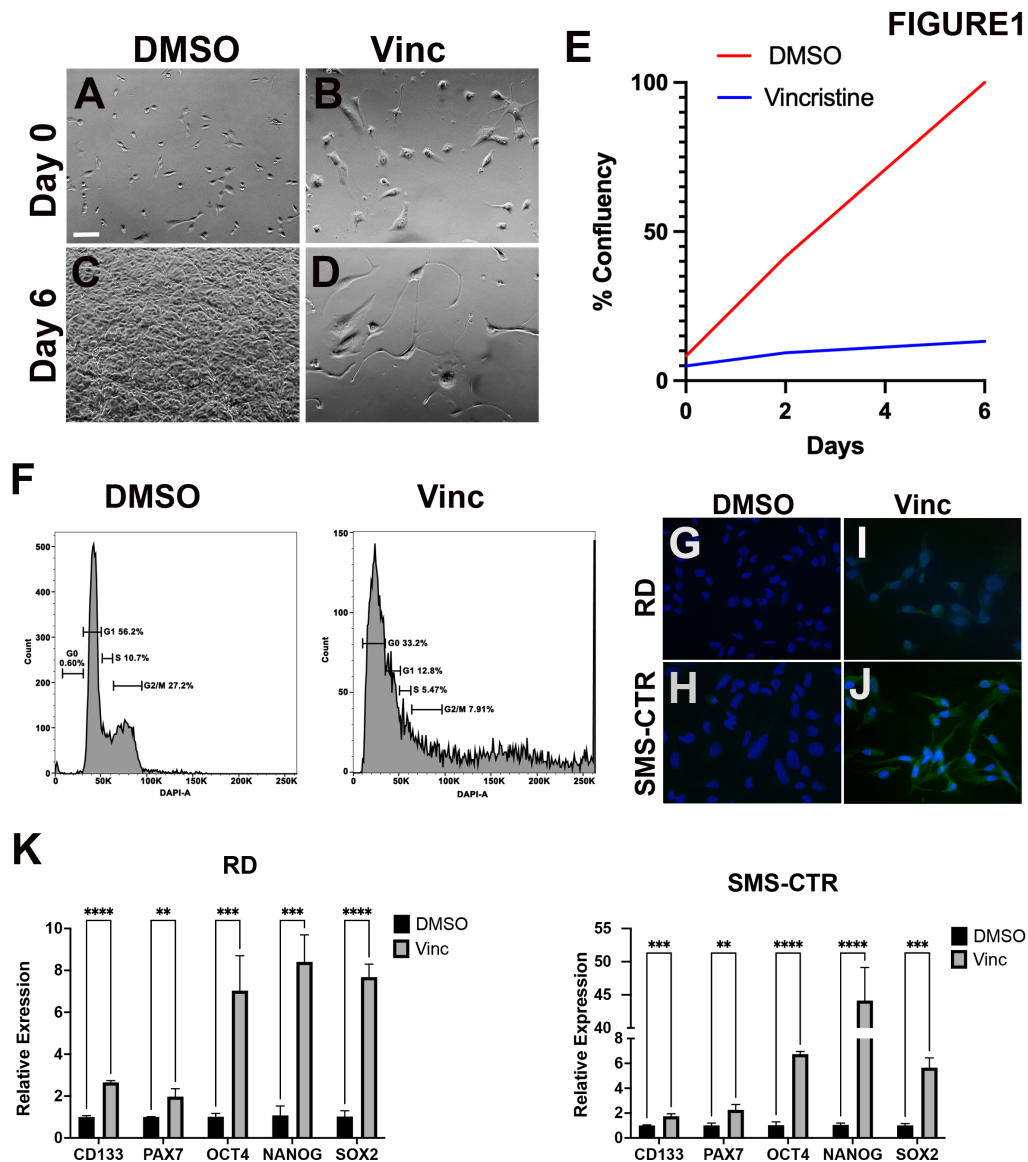
Figures

Figure 1

RMS-resistant cells in response to vincristine treatment show stem-like characteristics. (A-D) Representative bright-field images of RD cells treated with DMSO (vehicle) and continuous exposure of vincristine at 1 nM on day 0 (A-B) and day 6 (C-D). Magnification: 100x. Scale bar: 100 microns. (E) The changes in the percentage of confluence for the RD cells over 6 days as quantified using the ImageJ software. Shown is the results from one of the 3 independent experiments. (F) SMS-CTR cells treated with vincristine at IC 80-90 (1.5 nM) were fixed and stained with DAPI for cell cycle analysis by flow cytometry. Representative plots are shown for two representative samples from one of two independent experiments (G-J) Representative images of immunofluorescence (IF) against CD133 on RD and SMS-CTR DTPs following 10 days of vincristine treatment. DMSO vehicle-treated cells in (G-H), and vincristine-treated ERMS cells (2 nM for RD and 1.5 nM for SMS-CTR) in (I-J). FITC: CD133 staining; Blue: DAPI nuclear staining. (K) Quantitative RT-PCR on RD and SMS-CTR cells treated with either DMSO or vincristine (2 nM for RD and 1.5 nM for SMS-CTR) for 7 days. Error bar: standard deviation (STD) of 3 replicate samples. ** = $P < 0.01$; *** = $P < 0.005$; **** = $P < 0.0005$ by unpaired t-test.
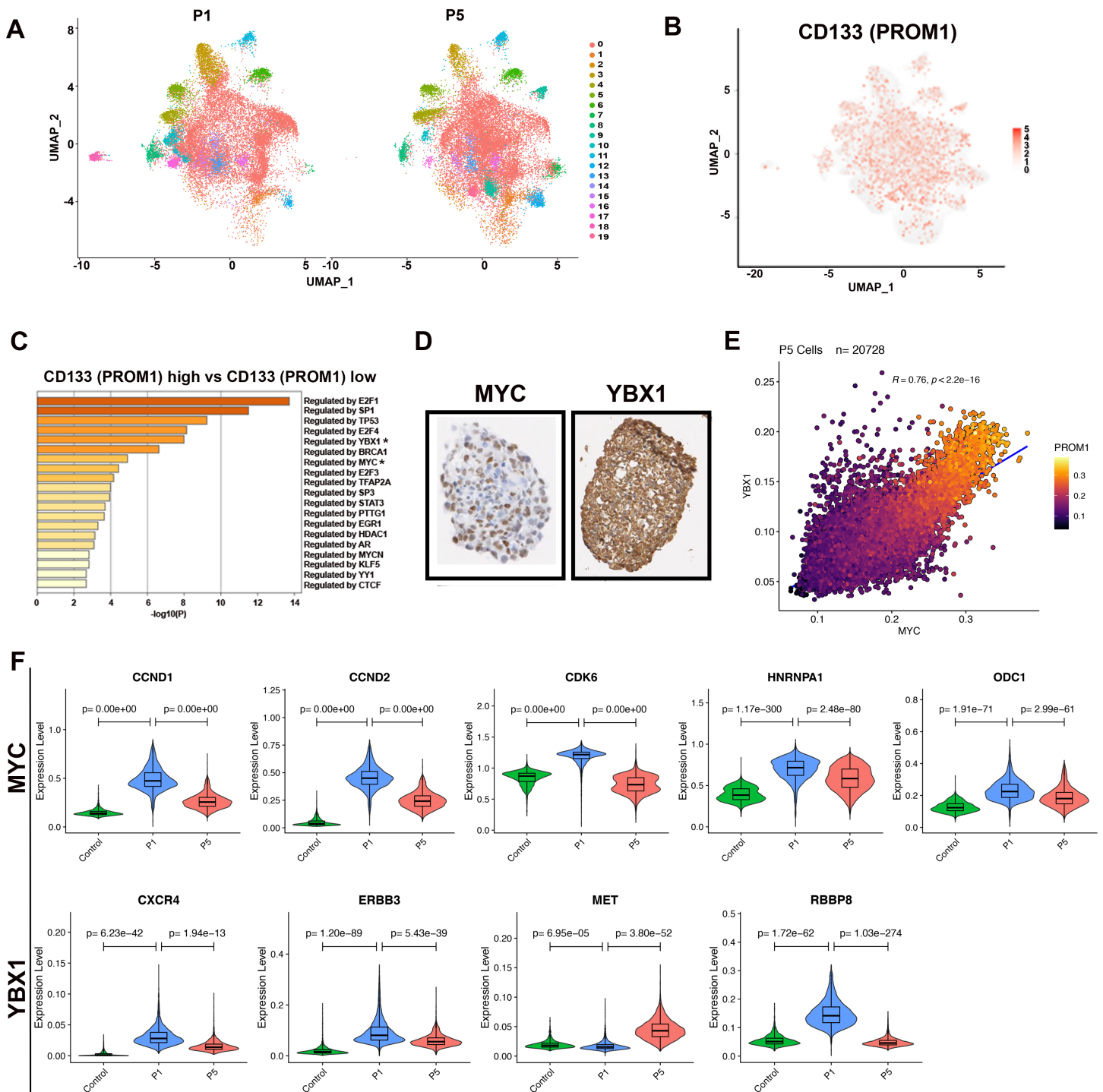
Figure 2

Figure 2

Single cell RNA sequencing expression analysis reveals MYC and YBX1 top regulators in CD133-high expressing ERMS cells. (A) UMAP demonstrates clustering of RD spheres from passage 1 (P1) and passage 5 (P5). (B) UMAP analysis for *CD133*(*PROM1*)-expressing cells in the RD sphere cells. (C) TRUUST analysis for top transcription factor-interacting regulators in *CD133* (*PROM1*) high-expressing sphere cells. (D) Immunohistochemistry assessing MYC and YBX1 protein expression in RD spheres from

P5. (E) Pearson correlation analysis on the relationship between MYC and YBX1 in RD sphere cells from P5. Heatmap indicates expression levels of CD133 in RD cells analyzed. (F) Violin plots showing gene expression level distribution of MYC and YBX1 target genes. Control: parental adherent cells.
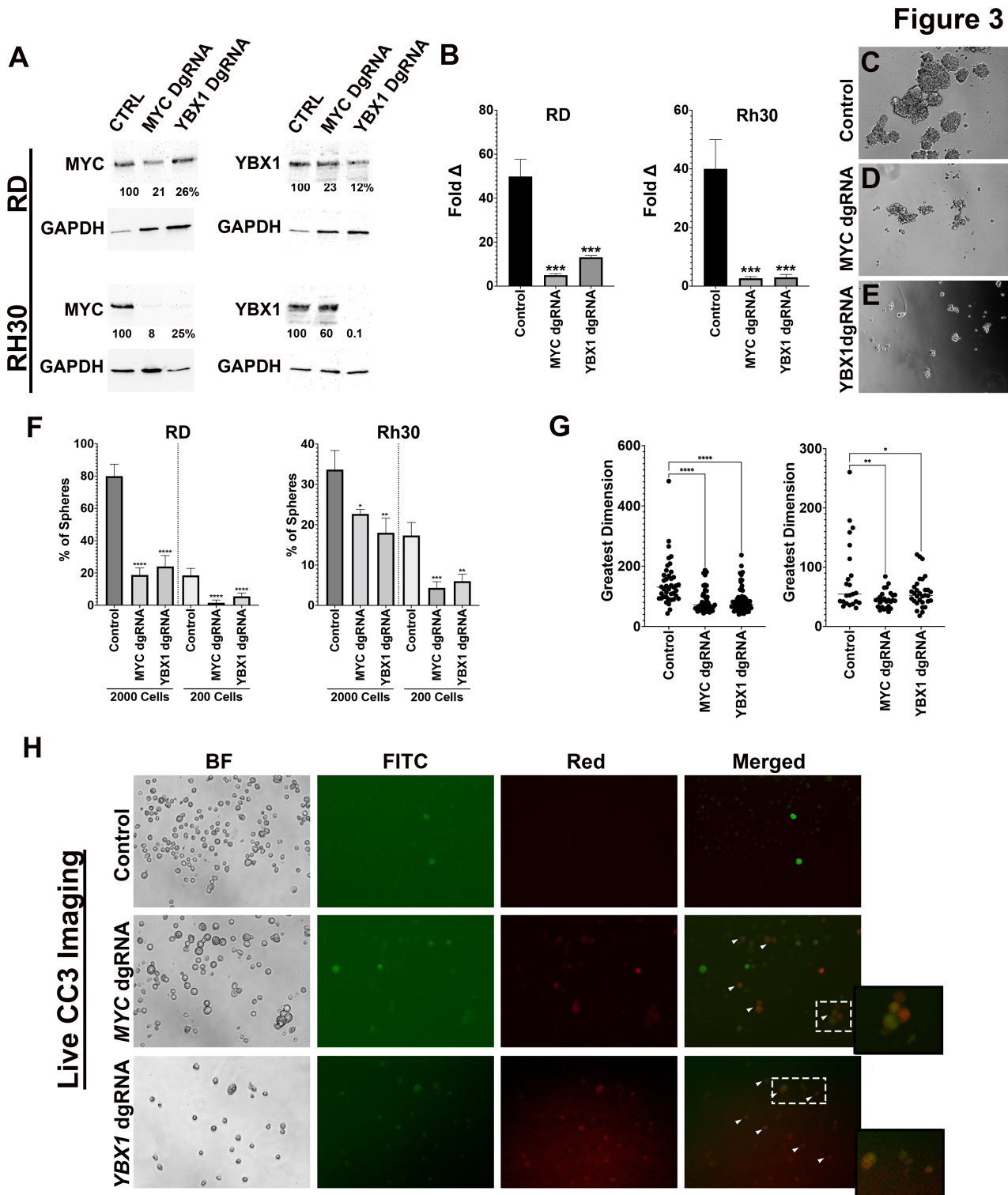

Figure 3

Targeted disruption of *MYC* or *YBX1* reduces RMS tumor cell growth and sphere formation. (A) Western blots against MYC and YBX1 in RD and Rh30 cells with CRISPR/Cas9-mediated disruption of *MYC* and *YBX1*. DgRNA = double gRNA. Ratio of band intensity relative to safe-harbor dgRNA control following normalization to GAPDH is shown below each band. (B) Cell counts of RD and Rh30 cells with CRISPR/Cas9-mediated disruption of *MYC* and *YBX1*. Stable Cas9-expressing RD and Rh30 cells were transduced with lentiviral CRISPR targeting constructs, and then plated 3 days post antibiotic selection. Cell counts were performed 6 days later. Cell counts were normalized to day 0. (C-E) Representative images of RD spheres from CRISPR/Cas9-mediated safe-harbor region targeting (control), *MYC* targeting and *YBX1* targeting. (F) Summary of limiting dilution sphere assays for RD and Rh30 cells that were plated at 2000 and 200 cells. (G) Summary of sphere size (greatest dimension) quantification as determined by the Image J software. (H) Representative images from live imaging using fluorogeneic NucViewÒ530 Caspase-3 substrate for detecting apoptotic cells. CD133:GFP SMS-CTR cells were stained with the substrate for 1 hour 5 days following lentiviral transduction of the CRISPR dgRNA constructs. BF: bright field. CD133:GFP expressing cells were detected using the FITC channel. The cells labeled with NucViewÒ530 Caspase-3 substrate were detected using the red channel. Arrow heads in the merged images indicate CD133-positive cells undergoing apoptosis. For panels B, F and G, error bar = STD of 3 replicate wells from 1 of 4 independent experiments. ns = not significant, * = $P < 0.05$; ** = $P < 0.01$; *** = $P < 0.005$; **** = $P < 0.0005$ by one-way ANOVA analysis with Dunnett's multiple comparisons' test.
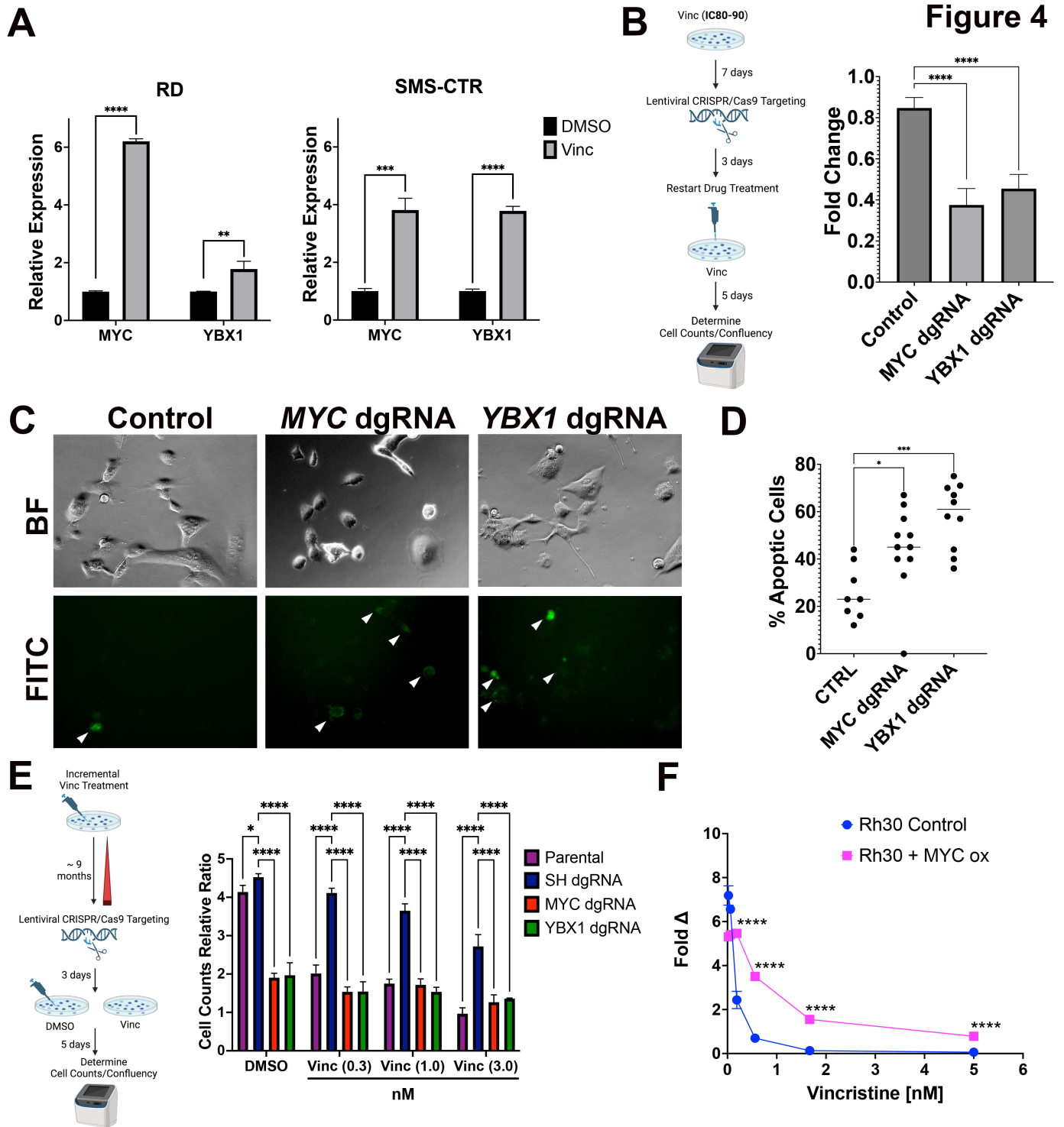
Figure 4

MYC and YBX1 are essential for maintaining viability of vincristine-tolerant RMS cells. (A) Summary of quantitative RT-PCR results comparing expression of *MYC* and *YBX1* in RD and SMS-CTR vincristine-resistant cells following 7-day treatment of vincristine at IC80 (1-1.5 nM). (B) Right panel: schematic of the experiment: RD vincristine-resistant cells generated from 7-day vincristine treatment at 2 nM were transduced with lentiviral CRISPR/Cas9 constructs against *MYC* and *YBX1*. Following transduction and selection, cells were exposed again to vincristine continuously for 6 days. Right panel: quantitative

summary of cell growth analysis. Fold change in cell counts over 6 days is shown for each condition. Safe-harbor region targeting control was used. (C) Representative images from live imaging using the fluorogeneic NucViewÒ488 Caspase-3 substrate for detecting apoptotic cells in RD cells. Cells were imaged 8 hours after starting vincristine treatment, and 1 hour of exposure to the substrate. (D) Quantitative summary of the results from the imaging study for apoptosis. For each condition, images were taken from at least 8-10 random fields at 200x magnification across 3 biological replicates. (E) Summary of vincristine dose-response results by the Cell-Titer Glo viability assays on the RD resistant cells generated from incremental exposure of vincristine until IC50 was 10 folds higher than that of the parental cells. Luminescence values were normalized to day 0. Right panel: experimental schematic; left panel: quantitative results. (F) Dose-response curves of a stable Rh30 cell line overexpressing MYC. GFP overexpression was used as the control. * = $P < 0.05$; ** = $P < 0.01$; *** = $P < 0.005$; **** = $P < 0.0005$ by unpaired t-test in A, one-way ANOVA in D and two-way ANOVA in B, E and F with Dunnett's multiple comparisons test.
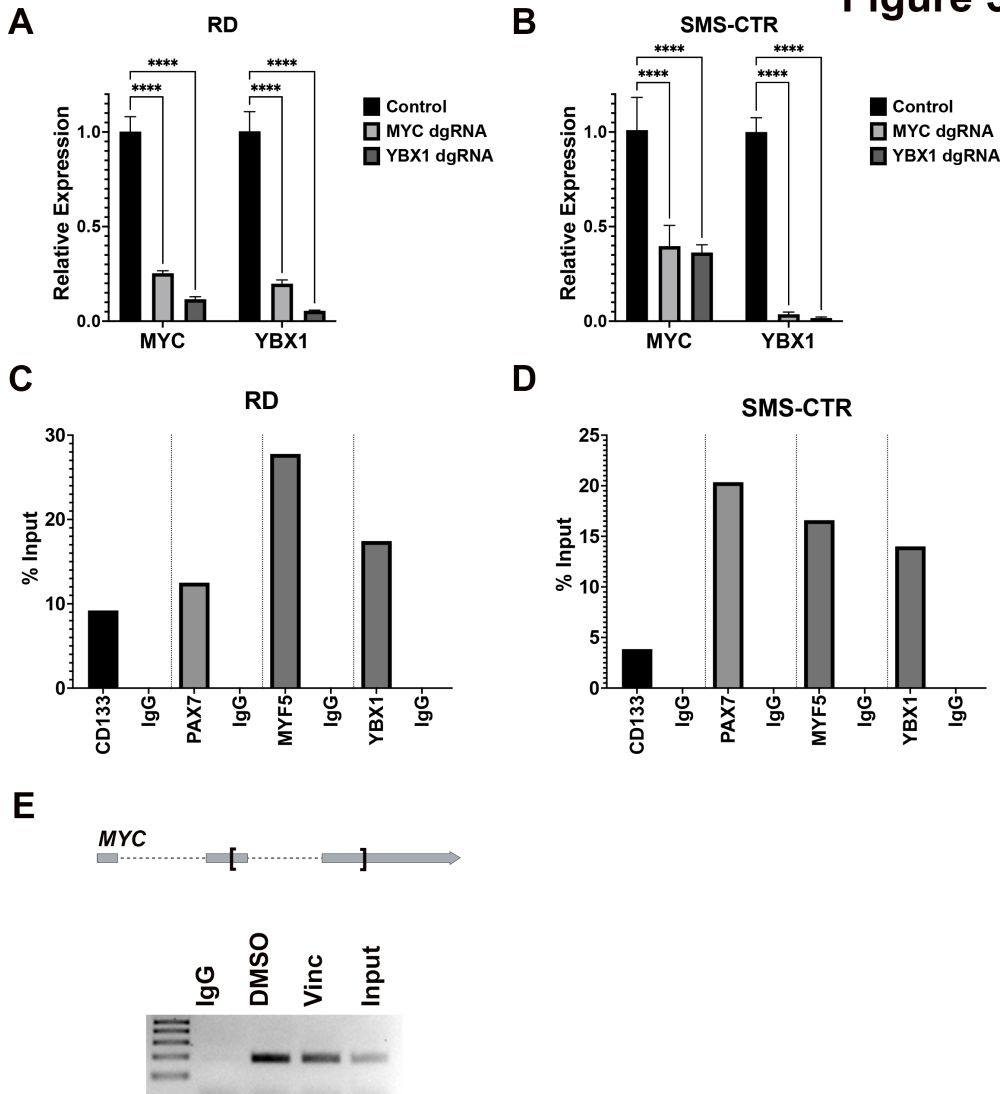
Figure 5

Reciprocal interaction of MYC and YBX1. (A-B) Summary of quantitative RT-PCR assessing expression of *MYC* and *YBX1* mRNA in RD and SMS-CTR cells with targeted disruption of *MYC* and *YBX1* (8 days post-transduction). (C-D) Summary of quantitative PCR following CUT&RUN reactions using the MYC antibody against the chromatin extracted from vincristine-treated C) RD and D) SMS-CTR cells. Anti-rabbit IgG was used as the negative control. Shown is the average of 3 replicate samples. (E) RNA immunoprecipitation

assay against YBX1. Shown is the gel electrophoresis results of quantitative RT-PCR products from RD cells using primers against *MYC*3'UTR. The regions in *MYC* mRNA amplified by PCR are indicated by the bracket in the schematic at the top of the panel.
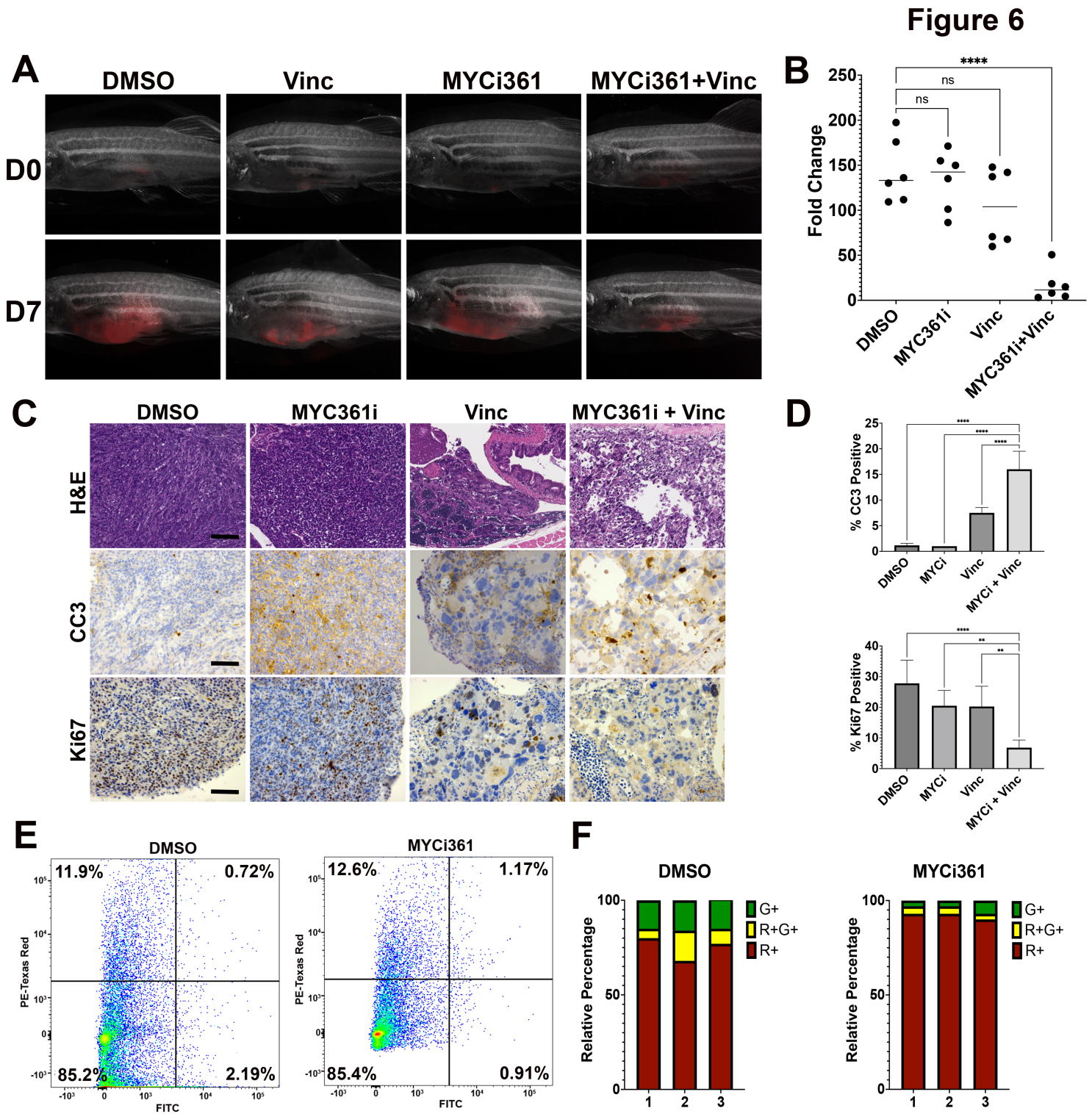

Figure 6

Treatment of zebrafish FN RMS tumors with MYCi361 results in reduced tumor growth and depletion of tumor-propagating cell population. (A) Representative images of mCherry-labeled KRASG12D-driven FN RMS tumor-bearing CG1-strain zebrafish treated with the vehicle DMSO, MYCi361 (100 mg/kg), vincristine (0.4 mg/kg) and the two-drug combination at day 0 and day 7. (B) Summary of tumor volume fold change over the 7-day treatment period. **** = P < 0.0001; ns = no significant by one-way ANOVA. (C) Representative images of H&E and immunohistochemistry (IHC) for cleaved caspase-3 (CC3) and Ki67 performed on tissue sections from zebrafish ERMS tumors treated with DMSO, MYCi361, vincristine and the two-drug combination. Scale bar: 500 microns. (D) Quantitation of CC3 and Ki67 images. % of positive cells was quantified over 3 fields at 400x magnification for each tumor section. The average of 6 fields total in two tumors for each condition is shown. ** = P < 0.01; **** = P < 0.0001 by one-way ANOVA with Dunnett's multiple comparisons test. (E) Flow cytometry analysis of fluorescence-labeled cell subpopulations [*myf5*:GFP-positive /*mylz2*:mCherry-negative (G+); *myf5*:GFP-positive /*mylz2*:mCherry-positive (G+/R+); *myf5*:GFP-negative)/*mylz2*:mCherry-positive (R+)] in zebrafish ERMS tumors treated with DMSO and MYCi361 (100 mg/kg). (F) Summary of relative ratios of tumor cell subpopulations. Each bar represents one fish.
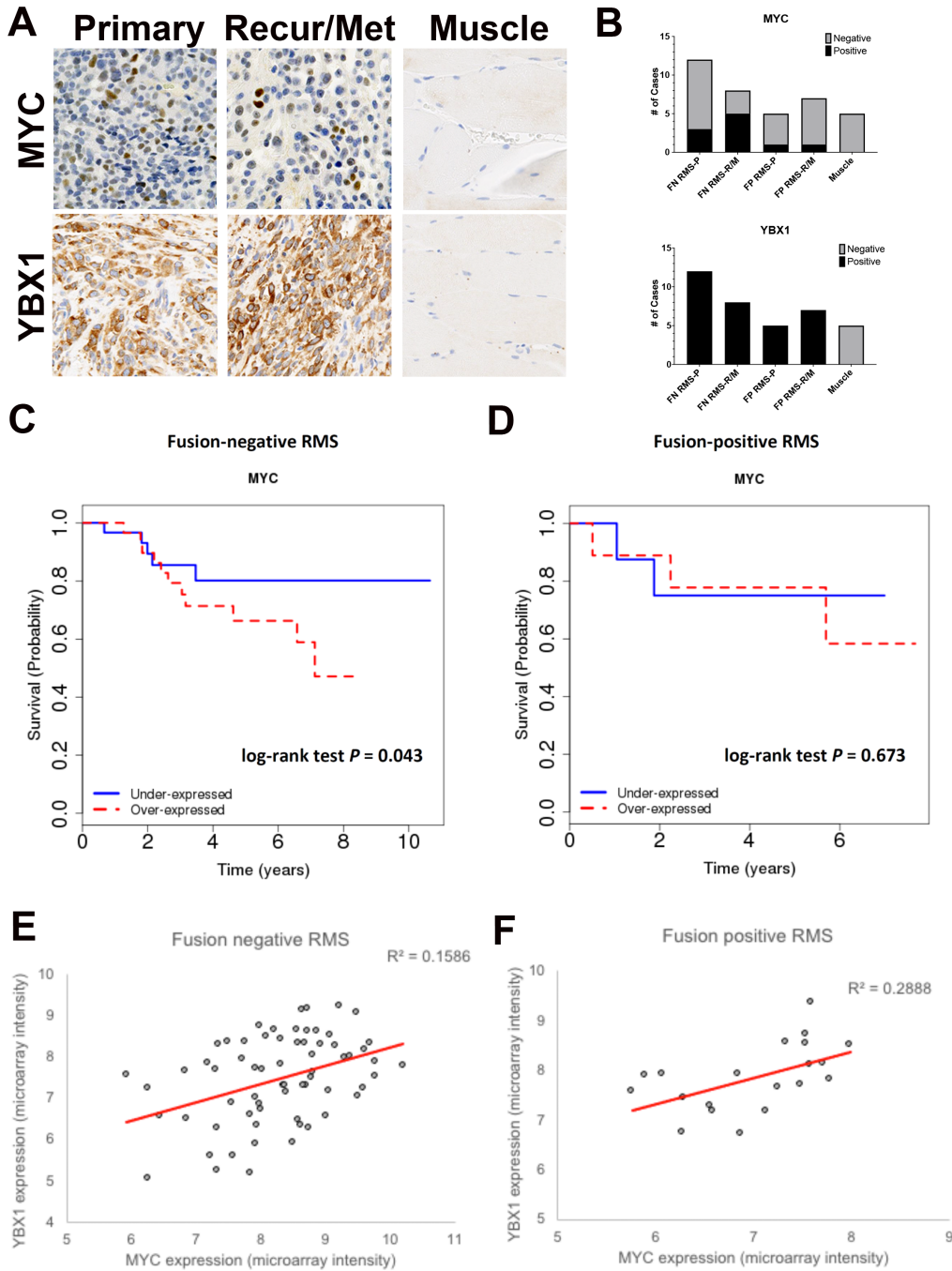
Figure 7

Figure 7

Expression of MYC and YBX1 in RMS with recurrent/metastatic disease and correlation with outcomes.
(A) Representative images of patient RMS (primary and recurrent or metastatic) and normal muscle tissue sections stained by IHC for MYC and YBX1. (B) Summary of IHC results in fusion-positive (FP) and fusion-negative (FN) RMS cases. (C-D) Pearson correlation analysis on MYC and YBX1 expression levels

in FN and FP RMS patients. Correlation coefficient for each comparison is shown. (E-F) Kaplan Meier analysis of high and low-expressing MYC FN and FP RMS cases.

Supplementary Files

This is a list of supplementary files associated with this preprint. Click to download.

- SuppFigsCombined.pdf
- SupplementalLegendsMethodsFinal.docx
- TableS11.docx